AJNR

Assessment of Craniospinal Arteriovenous Malformations at 3T with Highly Temporally and Highly Spatially Resolved Contrast-Enhanced MR Angiography

R.S. Saleh, D.G. Lohan, J.P. Villablanca, G. Duckwiler, S.T. Kee and J.P. Finn

Assessment of Craniospinal Arteriovenous Malformations at 3T with Highly Temporally and Highly Spatially Resolved Contrast-Enhanced MR Angiography

R.S. Saleh
D.G. Lohan
J.P. Villablanca
G. Duckwiler
S.T. Kee
J.P. Finn

BACKGROUND AND PURPOSE: Patients with arteriovenous malformation (AVM) are known to have an elevated risk of complications with conventional catheter angiography (CCA) but nonetheless require monitoring of hemodynamics. Thus, we aimed to evaluate both anatomy and hemodynamics in patients with AVM noninvasively by using contrast-enhanced MR angiography (CE-MRA) at 3T and to compare the results with CCA.

MATERIALS AND METHODS: Institutional review board approval and informed consent were obtained for this Health Insurance Portability and Accountability Act–compliant study. Twenty control subjects without vascular malformation (6 men, 18–70 years of age) and 10 patients with AVMs (6 men, 20–74 years of age) underwent supra-aortic time-resolved and high-spatial-resolution CE-MRA at 3T. Large-field-of-view coronal acquisitions extending from the root of the aorta to the cranial vertex were obtained for both MRA techniques. Image quality was assessed by 2 specialized radiologists by using a 4-point scale. AVM characteristics and nidus size were evaluated by using both CE-MRA and CCA in all patients.

RESULTS: In patients, 96.6% (319/330) of arterial segments on high-spatial-resolution MRA and 87.7% (272/310) of arterial segments on time-resolved MRA were graded excellent/good. MRA showed 100% specificity for detecting feeding arteries and venous drainage ($n = 8$) and complete obliteration of the AVM in 2 cases (concordance with CCA). Nidus diameters measured by both MRA and CCA resulted in a very strong correlation ($r = 0.99$) with a mild overestimation by MRA (0.10 cm by using the Bland-Altman plot).

CONCLUSION: By combining highly temporally resolved and highly spatially resolved MRA at 3T as complementary studies, one can assess vascular anatomy and hemodynamics noninvasively in patients with AVM.

Craniospinal arteriovenous malformation (AVM) typically presents in a young adult with intracranial hemorrhage (30%–82%), headache, seizures, or focal neurologic deficits that are either related to mass effect or to vascular steal phenomena.[1] Hemorrhage occurs with an annual incidence of 2%–4%[2,3] and remains the prime vector for mortality and morbidity (10% and 16%–50%, respectively).[4-6] Several investigators have identified features predictive of hemorrhage, including small nidus size, deep nidus location, single deep venous drainage, associated arterial aneurysm, impaired venous drainage, and high intranidal pressure.[7-10] Safe and accurate diagnostic work-up is essential to provide an architectural map and to define hemodynamic indices and risk predictors. Moreover, follow-up studies may be required for monitoring posttherapy. The current gold standard for assessment of AVM is conventional catheter angiography (CCA), which is associated with ≤1.3% of major complications and death (<0.1%).[11-13] In this context, multiple catheter examinations in patients with AVM are expected to elevate the risk of complications and hemorrhage.

Recent advances in the performance of contrast-enhanced MR angiography (CE-MRA) at 3T have underscored its growing potential for detailed evaluation of the supra-aortic arteries and veins.[14-16] Techniques have been established for both highly temporally resolved and highly spatially resolved CE-MRA, by using only modest contrast doses.[17,18] Whereas high-spatial-resolution MRA can quickly provide detailed images of intracranial and extracranial vessels, time-resolved MRA adds hemodynamic information and can capture transient processes, such as early venous filling, which is the hallmark of an arteriovenous fistula (AVF).[17,19] Moreover, cortical venous reflux has a high yearly risk of hemorrhage[20-24] and influences treatment.[24-28] Micro-AVMs as a potential source of fatal intracranial hematoma represent approximately 8%–10% of surgically treated brain AVMs.[29,30] Time-resolved MRA may potentially identify an early filling vein in a micro-AVF because the anatomy of a very small nidus may not be assessable. Furthermore, an early filling vein may be the only evidence of a residual shunt after radiosurgery or endovascular therapy.

These 2 approaches can, therefore, provide complementary diagnostic information to each other for evaluation of high-flow AVMs. The purpose of our study was to evaluate the potential of these complementary modes in defining the relevant vascular anatomy and hemodynamics noninvasively in patients with AVM and to compare the findings with those on digital subtraction angiography (DSA).

Methods and Materials

Patients

Our Health Insurance Portability and Accountability Act–compliant study was approved by the institutional review board, and informed consent was obtained from all subjects. Between April 2005 and July 2007, 10 consecutive patients (6 men/4 women; mean age, 41.7 ± 20 years; range, 20–74 years) with known vascular malformations were referred for clinical MR imaging and were prospectively enrolled in the study (9 patients with AVMs and 1 patient with AVF). All patients had undergone concurrent CCA and MRA: 6 patients had undergone MRA after treatment and 4 had MRA at the time of initial diagnosis.

For comparative analysis of image quality, 20 consecutive subjects as controls, with no vascular abnormality and no known diseases (6 men/14 women; mean age, 50 ± 17 years; range, 18–70 years), were identified. All subjects were scanned with the same protocol by using both high-spatial-resolution CE-MRA and dynamic time-resolved CE-MRA, as detailed below.

Imaging Techniques

MR Imaging Protocol. All cerebrospinal MRA studies were performed on a 32-channel 3T whole-body MR imaging system (TIM Trio; Siemens Medical Solutions, Malvern, Pa). A total of 22 independently channeled coil elements were activated, including a 12-channel head matrix coil, a 4-channel neck coil, and a 6-channel spine coil. These coils encompassed a sensitive volume, which included the upper thorax, cervical spine, and cranium. Patients were positioned supine on the scanner table and advanced head-first into the magnet bore. To define the appropriate timing for high-spatial-resolution CE-MRA, we performed a sagittal timing acquisition, by using a 3D T1-weighted gradient-recalled echo (GRE) sequence (TR/TE, 2/1 ms; flip angle, 15°) during the injection of 2-mL gadopentate dimeglumine (Magnevist; Berlex Laboratories, Wayne, NJ) at a rate of 1.2 mL/s and flushed with 20-mL saline. The 3D dataset was updated every 1.1 second, during 35–40 seconds of quiet breathing.

Dynamic Time-Resolved MRA. For time-resolved angiography, an ultrafast 3D GRE sequence[17] was used (following the sagittal timing run). A coronal 9-cm slab was acquired by selecting a section thickness of 4 mm and 24 partitions, over a 500-mm FOV (the upper thorax to the cranial vertex). Twelve to 16 sequential measurements were acquired during a 20- to 25-second breath-hold, while injecting 4 mL of contrast at a rate of 3 mL/s followed by 20 mL of saline flush. Sequence parameters were TR/TE, 2.6/1.1 ms; flip angle, 18°; bandwidth, 750 Hz/pixel; and voxel size, $1.2 \times 1 \times 4$ mm^3. Generalized autocalibrating partially parallel acquisition (GRAPPA × 3) was used in the right-left phase-encoding direction. Scanning delay was determined on the basis of the timing-run images. Maximum intensity-projection (MIP) reconstruction was performed in-line. To further reduce acquisition time, we applied phase and section partial Fourier (6/8) with zero interpolation, resulting in 1.5-second 3D acquisitions.

High-Spatial-Resolution CE-MRA. Following the time-resolved acquisition, single-phase high-spatial-resolution CE-MRA of the carotid and vertebrobasilar circulation was performed with the following parameters: TR/TE, 3.1/1.1 ms; flip angle, 20°; bandwidth, 720 Hz/pixel; 0.15 mmol/kg of contrast was injected at a rate of 1.2 mL/s followed by a 30-mL saline flush. A coronal acquisition was used with a 450-mm FOV on a 640 matrix in the frequency-encoding direction by using 120 partitions (voxel size, $0.8 \times 0.7 \times 0.8$) during a 22-second breath-hold.[14] Parallel acquisition was used (GRAPPA × 4) in the right-left phase direction with 24 reference lines. To further min-

imize acquisition time, we used partial Fourier (6/8) in both phase and section directions, by using a linear k-space acquisition. Data acquisition was timed to coincide with peak aortic filling, based on the test injection.

Postprocessing and Image Analysis

After data acquisition, image processing was performed on a 3D workstation (Leonardo; Siemens Medical Solutions), with standard commercial software by using MIP and volume-rendering (VR) algorithms. Overlapping thin MIP subvolumes (10 mm, with 9 mm overlap) in the coronal, sagittal, and axial planes (or any desired obliquity, if so requested by observers for better assessment of targeted structures) were reconstructed for all source images. In addition, full-volume MIP reconstructions over a 360° rotated range and 3D VR images were generated on the same workstations, either for full or selective subvolume assessment of the 3D dataset.

CCA

CCA (Integris V, Philips Medical Systems, Best, the Netherlands) images were acquired with multiple superselective manual injections (a total of 100–170 mL) of contrast (Omnipaque 300; GE-Amersham Healthcare, Princeton, NJ) administered at 5 mL per selection. Digitally subtracted images from these injections in both the arterial and venous phases, in anteroposterior, lateral, and oblique views, were recorded. CCA was performed with a 15-mm FOV and a matrix of 1024×1024, in which magnification factors were accounted for on assessment of nidus architecture, arterial feeders, and outflow vasculature.

Image Analysis

Image-Quality Analysis: High-Spatial-Resolution MRA. The following 33 arterial segments were assessed for image quality in subjects with AVM: aortic arch; brachiocephalic trunk; bilateral subclavian arteries; common, external, and internal carotid arteries (cervical, petrous, cavernous, and supraclinoid segments); anterior cerebral arteries; middle cerebral arteries (MCA, comprising 3 segments: MCA 1 [horizontal], MCA 2 [Sylvian], and MCA 3 [cortical]); vertebral arteries; posterior inferior cerebellar arteries; posterior cerebral arteries; superior cerebellar arteries; and the basilar artery. Overall image-quality analysis was performed independently by a neuroradiologist and a cardiovascular radiologist with 12 and 4 years' experience, respectively. The reviewers evaluated the images without access to clinical data, with regard to arterial enhancement and the presence of artifacts (including parallel acquisition reconstruction artifact and motion artifact) by using a 4-point grading system as follows:

- 1. Indicates excellent image quality and arterial enhancement with a very high level of confidence in diagnostic content.
- 2. Indicates good image quality and arterial enhancement, adequate for confident diagnosis.
- 3. Indicates fair image quality, but inadequate arterial enhancement for confident diagnosis.
- 4. Indicates poor image quality and blurring of the arterial segment or not seen.

Additionally, AVM characteristics were assessed by using processed data and source data as follows:

- Assessment of arterial feeder/feeders: readers were asked to identify the feeding artery/arteries.
- Nidus evaluation: maximal orthogonal diameters of nidus, nidus

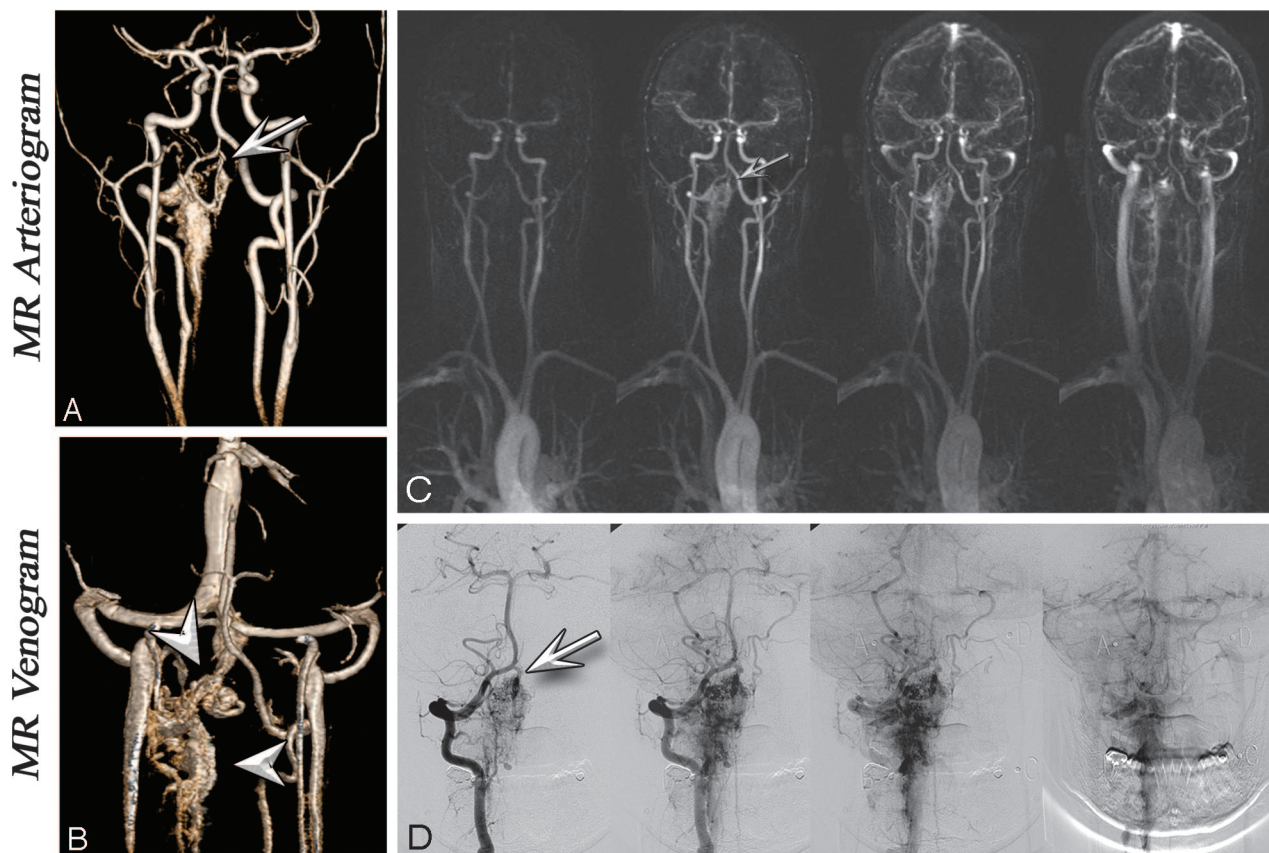**Fig 1.** *A* and *B*, Coronal VR projections from CE-MRA (voxel volume, 0.8 × 0.7 × 0.8 mm³) in a 22-year-old woman with a history of intraspinal hemorrhage and cervical laminectomy. Arterial (*A*) and venous (*B*) phase images show a diffuse serpiginous cervical C2–C3 AVM. Note the feeding vessel derived from the right vertebral artery (*arrows*). Venous drainage was through the paravertebral venous plexus and the occipital sinus (*arrowheads*). *C*, Time-resolved images with 1.5-second temporal resolution and 1.2 × 1 mm in-plane resolution show enhancement of the AVM via the right vertebral artery (*arrows*) and subsequent venous drainage. *D*, A phase-by-phase comparison with CCA is presented. MRA and CCA examinations were performed on the same day, before radiosurgery.

configuration (compact, diffuse, or multicompartmental), presence of nidal aneurysm or AVFs.

- Efferent vessels assessed for drainage: deep or superficial and presence of anterograde or retrograde flow in the venous phase.

The definition of the feeding artery and efferent vein was assessed by using a 3-point grading system:

- One indicates excellent visualization of the feeding artery/efferent vein, with clear relationship (70%–100% confidence) to the AVM nidus.
- Two indicates intermediate-quality visualization of the feeding artery/efferent vein (40%–69% confidence of relationship to the nidus).
- Three indicates poor recognition of the feeding artery/efferent vein, with no clear relationship (<40% confidence) to the nidus.

Image-Quality Analysis: Dynamic Time-Resolved MRA. For qualitative assessment, overlapping thin MIP (10-mm thickness by 9-mm overlap) reconstructions of the peak arterial enhancement phases were reviewed for both patients with AVM and control subjects. Using the same scoring system as the high-spatial MRA, we additionally assessed all arterial segments by using time-resolved MRA, except for the bilateral supraclinoid segment of the internal carotid artery (31 segments for each subject).

Additionally, by using MIP projections of time-resolved MRA, we assessed hemodynamic processes such as sequential filling of the feed-

ing artery, nidus, early enhancement of venous drainage, presence of venous reflux, or any retrograde flow for patients with AVM.

CCA
All patients had concurrent CCA studies, which were compared with MRA. Two readers evaluated CCA studies in different sessions, blinded to patient information and clinical history. CCA images were assessed with regard to identification of arterial feeders, venous drainage, and maximal nidus diameters.

Statistical Analysis
MRA image-quality scores were ranked and listed as mean ± SD. The Pearson correlation test was used to show correlation between MRA and CCA for nidus size. The Bland-Altman test was used to show the difference between AVM size measured by both MRA and CCA. Comparison of image quality between patients with AVM and the control group was performed by using an unpaired nonparametric Mann-Whitney *U* test. For all comparison measurements, the level of significance was set at a *P* value < .05.

Results

Image Quality
Of 330 arterial segments assessed in patients with AVM with high-spatial-resolution MRA, 96.6% (319/330) were scored
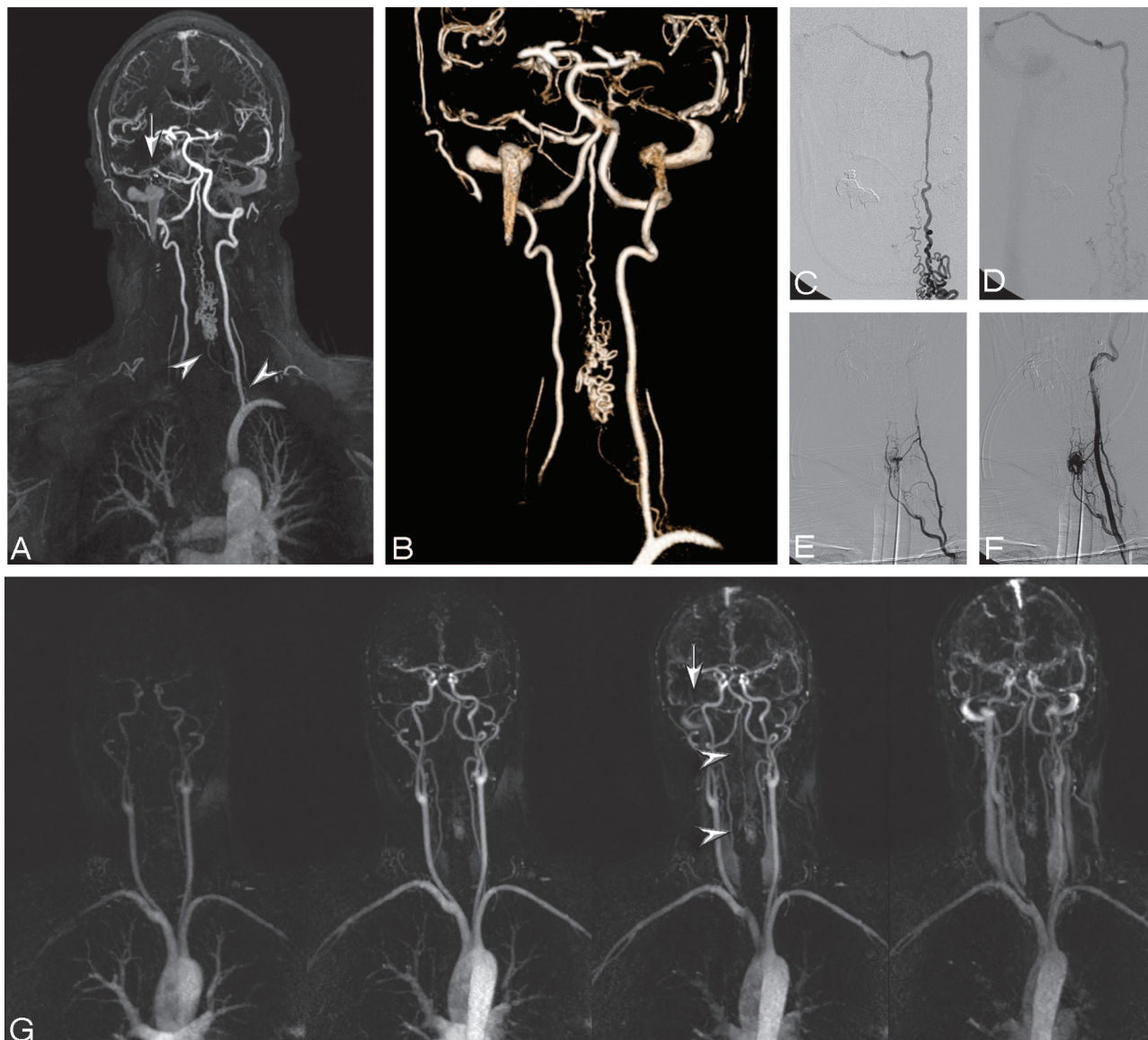
Fig 2. *A*, MIP from 3D high-spatial-resolution CE-MRA (voxel volume, 0.8 × 0.7 × 0.8) in a 43-year-old male patient with cervical AVM extending from C2 to C6. Note the left ascending cervical artery originating from the left thyrocervical trunk (*arrowheads*), appearing to course in a superior direction to feed the intramedullary AVM. This nidus drains via a prominent spinal vein into the right superior petrosal vein and into the right transverse sinus (*arrow*). *B*, VR reconstruction from high-spatial-resolution MRA. *C* and *D*, CCA of venous drainage. Note due to the small FOV, venous drainage is obtained by using separate injections. *E* and *F*, Superselective CCA from a thyrocervical trunk injection shows results consistent with those seen at MRA. *G*, Time-resolved MRA shows the nidus (*arrowheads*) and the draining vein (*arrow*).

within the diagnostic range (mean, 1.1 ± 0.4). In the control group, 98% (651/660) of arterial segments were in the diagnostic range (mean, 1.06 ± 0.4). No significant difference was detected by using a nonpaired nonparametric test (Mann Whitney *U* test, *P* > .05). Image-quality assessment for time-resolved MRA in patients with AVM showed 87.7% (272/310) at the diagnostic level, including scores 1 and 2 (mean, 1.3 ± 0.8). On time-resolved MRA of the control group, 89.5% (556/620) of vessels were within the diagnostic range (mean, 1.3 ± 0.7). Again, no significant difference was detected between the image quality in patients with AVM, when compared with that of the control subjects (*P* > .05). The overall interobserver agreement for qualitative analysis of MRA images was excellent (*κ* = 0.8; 95% confidence interval [CI], 0.7–0.82).

Time-resolved MRA showed sequential filling of the feed-

ing artery, nidus, and early enhancement of venous drainage in all patients, except for 2 posttreatment patients in whom no AVM residuum was present. One patient with a left posterior fossa AVF (fed by 2 branches of the external carotid artery to the left sigmoid sinus) had a left sigmoid sinus stenosis with retrograde flow from left-to-right sigmoid sinus and extensive collateral drainage through the paravertebral veins. Two other patients, 1 with right-occipital and the other one with right-parietal AVM, showed venous reflux to the superior sagittal sinus. A patient with spinal AVM had drainage through the paravertebral venous plexus.

Visualization scores on high-spatial-resolution MRA for feeding arteries and efferent veins at the AVM nidus showed means of 1.4 ± 0.8 and 1.1 ± 0.3, respectively. MR imaging findings in all 10 patients with concurrent CCA were concordant with CCA findings, including 2 patients with complete
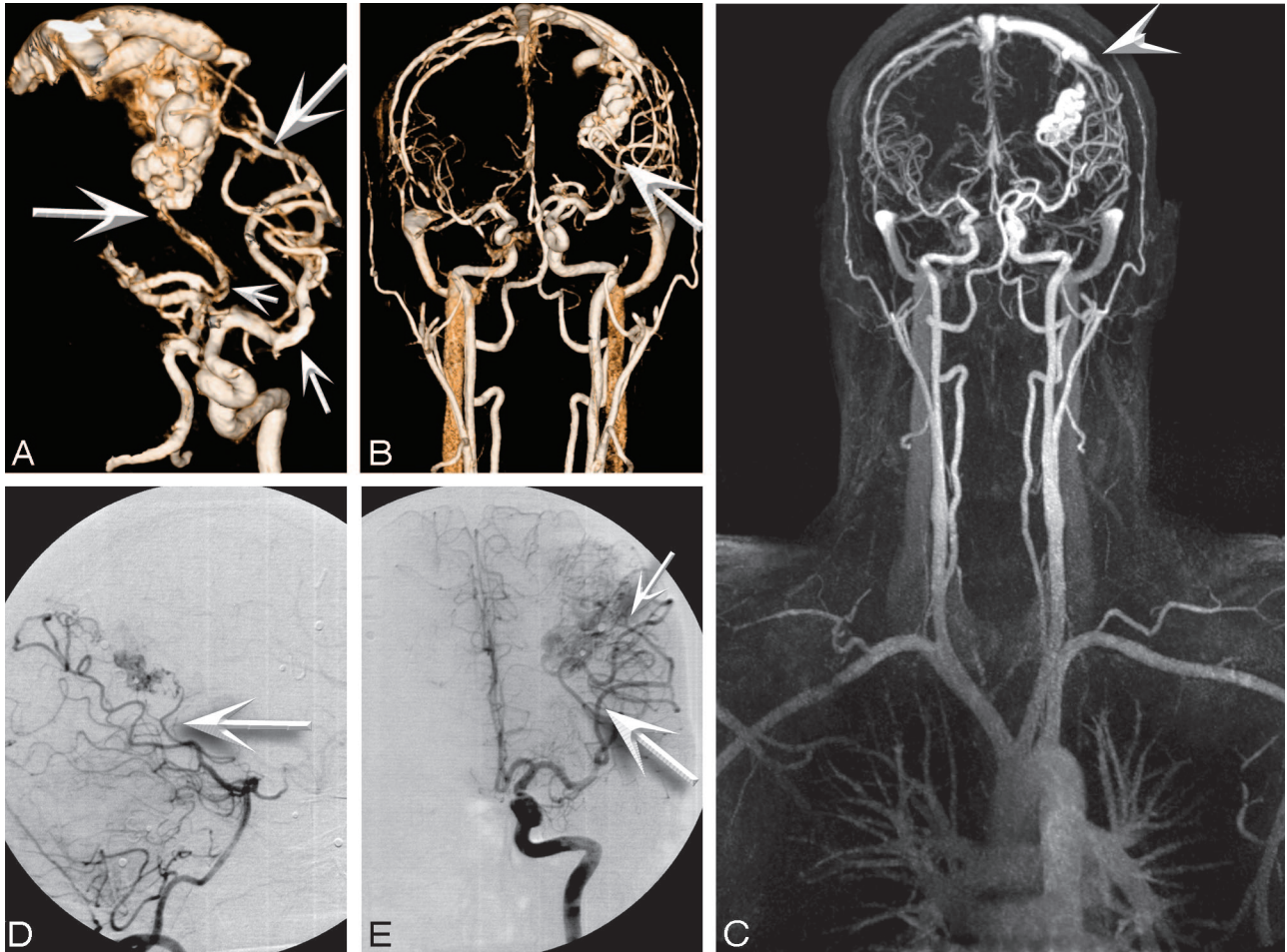
Fig 3. A 27-year-old man status postembolization and radiosurgery for a left parieto-occipital AVM in 2003 who presented for follow-up study and assessment for repeat radiosurgery. *A–E*, High-spatial-resolution MRA images and corresponding CCA images are as follows: right lateral oblique (*A*) and coronal 3D VR images (*B*), coronal full-volume MIP (*C*), lateral projection from superselection and angiogram of the basilar artery (*D*), and coronal view from superselection and angiogram of the left internal carotid artery (*E*). Feeder arteries are identified by both techniques as angular branches of the left MCA and parieto-occipital branches of the left posterior cerebral artery (*arrows*). Single venous drainage into the superior sagittal sinus is identified by both techniques (*arrowhead*).

obliteration of AVM after therapy (Table). All feeding arteries and draining veins were detected (grade 1 and 2) on MRA by both readers ($\kappa = 0.73$), yielding 100% specificity (Figs 1–4).

Nidus diameters measured by both techniques resulted in a very strong correlation ($r = 0.99$, $P < .0001$; with 95% CI for $r = 0.97$–0.99). Using a Bland-Altman agreement plot showed a mild overestimation (mean difference, 0.10 ± 0.5 cm) of diameter measurements by MRA.

Discussion

The results indicate that highly temporally resolved and highly spatially resolved MRA at 3T provide complementary information to each other about the vascular status of craniospinal AVMs. In our study, high-spatial-resolution MRA, coupled with time-resolved MRA, clarified the relevant vascular architecture and hemodynamics of cerebrospinal AVMs. High-spatial-resolution MRA showed excellent correlation with CCA ($r = 0.99$) for nidus size, with 100% visualization of feeding arteries and draining veins. When time-resolved MRA (voxel dimensions, $1 \times 1.2 \times 4$ mm^3) was insufficient to assess small arterial structures (eg, posterior inferior cerebellar arteries and/or superior cerebellar arteries), these vessels were clearly

visible on high-spatial-resolution MRA. However, in our study, none of these arteries contributed to the AVM.

To our knowledge, this is the first report applying time-resolved and high-spatial-resolution MRA to cerebrospinal AVMs to evaluate both anatomy and hemodynamics at 3T. Warren et al[31] used a dynamic 2D protocol (MR-DSA) in 3 orthogonal planes at 1 frame/s. Unlu et al[32] compared CE-MRA and time-of-flight MRA at 1T with CCA. They cited low spatial resolution, insufficient for detection of small AVMs, as the major limitation of their study. Meckel et al[33] reported a comparative study in which they used parallel acquisition (GRAPPA $\times$ 6) to acquire near-isotropic ($2 \times 2 \times 2.2$ mm^3) time-resolved MRA (FOV, 256×256; matrix, 128×128) at 1.5T during a 40-second acquisition time. Their work allowed a free-form interrogation of the 3D datasets; however, their spatial resolution remained limiting. In our study, patients held their breath during acquisition of the MRA, to eliminate motion artifact.[19] This is particularly relevant in the case of spinal AVM. Multichannel coil arrays and parallel imaging at 3T made possible detailed evaluation of dynamic vascular anatomy over an FOV encompassing the entire head and cervical spine. Because we used a fine imaging matrix (640) for
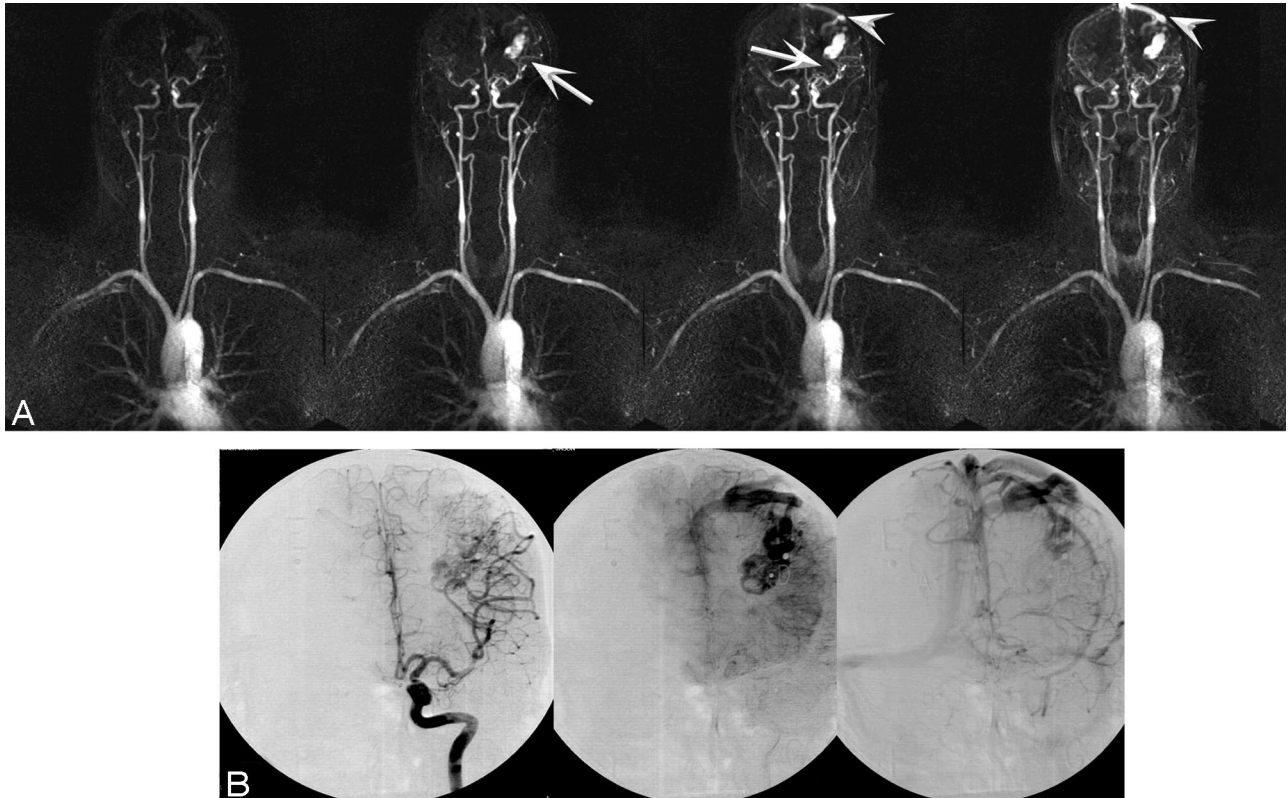
Fig 4. *A*, Time-resolved images with 1.5-second temporal resolution and 1.2 × 1 mm in-plane resolution from the same patient as in Fig 3. *B*, Coronal projection from the left internal carotid artery superselection and angiogram. Note sequential enhancement of the feeding arteries (*arrows*) and draining vein (*arrowheads*) by both techniques.

Characteristics of AVM based on MRA studies (concordant with CCA)†

		MRA Findings				CCA
No.	Location of AVM	Feeding Artery	Venous Drainage	Nidus Diameters (cm)	Nidus configuration	Nidus Diameters (cm)
1	Left parietal-occipital	MCA 2	SSS	13.5 × 2.5 × 1.75	Compact	11.5 × 2.7 × 1.5
2	Right occipital	PCA	Straight S and SSS	1.9 × 1.5 × 2.7	Diffuse	1.9 × 1.6 × -‡
3	Left temporal	PCA and MCA 2	Galen vein and SSS	4.9 × 5.2 × 6.0	Compact	4.5 × 5.2 × 6.2
4	Left posterior fossa AVF	Left external carotid (occipital branch and posterior auricular)	LSS	No nidus	No nidus	No nidus
5	Right parietal AVM	MCA 1	SSS	2.07 × 1.5 × 2.29	Compact	2.25 × 1.66 × 2.11
6	Cervical AVM (C2–C5)	Left subclavian	Ant. spinal V	4.8 × 1.8 × 0.7	Diffuse	4.9 × 1.8 × 0.7
7	Cervical AVM (C2–C5)	Right vertebral and ASA	RSS, straight S, and SSS	3.6 × 1.2 × 2	Compact	3.45 × 1.6 × 1.84
8	Cervical AVM (C1–C2)	ASA	Galen vein	1.1 × 1.1 × 2.0	Compact	1.6 × 0.8 × 1.6

Note:—PCA indicates posterior cerebral artery; ASA, anterior spinal artery; straight S, straight sinus; SSS, superior saggital sinus; LSS, left sigmoid sinus; Ant. spinal V, anterior spinal vein; RSS, right sigmoid sinus; AVF, arteriovenous fistula; AVM, arteriovenous malformation; MCA, middle cerebral artery. No residual AVM was detected after treatment on both MRA and CCA for patients 9 and 10.

high-spatial-resolution MRA, extended spatial coverage (head and spine) did not compromise voxel dimensions or imaging time.

Patients with AVMs may have coexistent vascular anomalies that increase the complexity of their treatment. Aneurysms may occur in 6.4%–55.6% of patients with AVMs[34,35] in vessels remote from the primary lesion or anywhere within the AVM nidus, feeding artery, or draining vein. Large FOVs can be advantageous in this context. Additionally, our study showed that large-FOV CE-MRA provided diagnostic infor-

mation comparable with that of multi-injection CCA in extensive AVM lesions (Fig 2). CCA provides 2D projectional images acquired through multiple superselective injections over a limited FOV (in our experience 15 cm in CCA versus 50 cm for MRA), which can limit assessment of the entire AVM territory. However, selective injection can also provide localized information not available in any other way. Therefore, the careful consideration of risk/benefit is appropriate when deciding if CCA is warranted in a specific case.

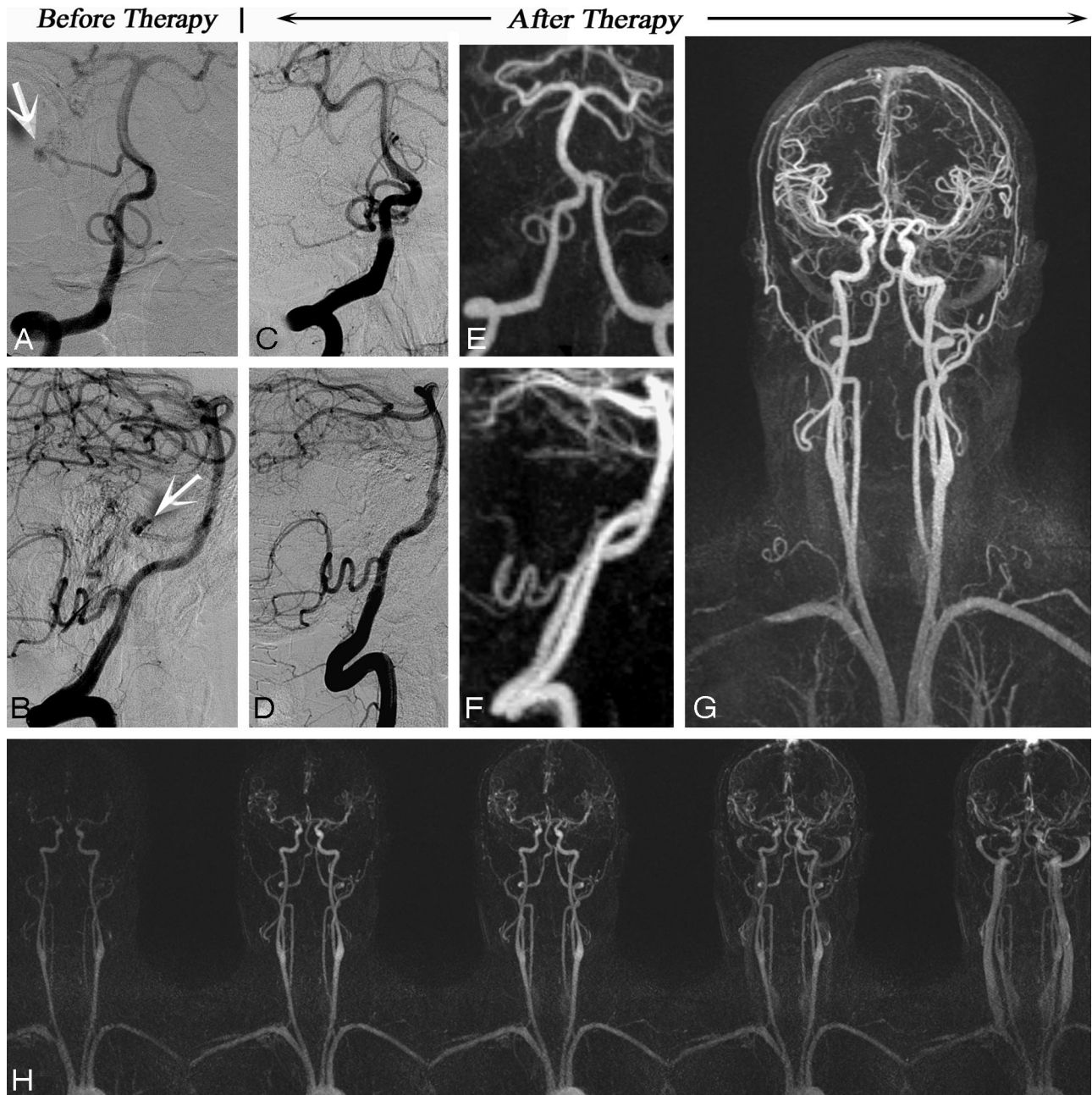Our results are encouraging. The high detection rate for

Fig 5. A 51-year-old male patient with subarachnoid hemorrhage and right cerebellar AVM who underwent surgical resection of an AVM. A and B, Coronal view from superselection and angiogram of the left vertebral artery (A) and its lateral projection (B) before therapy shows the AVM nidus (*arrows*). Follow-up CCA (C, coronal view and D, lateral projection) and follow-up MRA (E–H) images demonstrate complete obliteration of the AVM and no evidence of early draining vein. Corresponding high-spatial-resolution MRA and time-resolved images are as follows: coronal view of posterior circulation (both vertebral arteries) (E), saggital view (F), coronal full-volume MIP (G), and time-resolved MRA (H). MRA confirms the complete obliteration of the AVM.

AVM nidus, arterial feeder, and draining veins and the strong correlation with CCA for nidus size ($r = 0.99$) are promising.[32,36]

Dynamic information can further change the management of patients with dural AVF. The presence of venous reflux and retrograde flow is associated with higher pressure and risk of hemorrhage and progressive neurologic deficit due to venous congestion. This information is generally overlooked with static MRA, whereas time-resolved MRA could detect such dynamic processes. In our study, 2 patients with AVM and enlarged cortical venous drainage had retrograde flow in the superior sagittal sinus, and 1 case with AVF showed retrograde

flow in the left sigmoid sinus. Additionally, an early-filling vein may be the only sign of a residual shunt following treatment, which can be detected by using time-resolved MRA. In this study, 2 patients showed no residuum of AVM and early venous enhancement after therapy (Fig 5).

Our study has other limitations. The standard of clinical care at our institution is to use CE-MRA whenever possible in place of CCA, to limit patient exposure to the risks of catheterization and radiation, which limited to 10 the number of our subjects with correlative DSA; another 9 who had CE-MRA were excluded on this basis. Furthermore, we were not able to calculate sensitivity in our study because most of our

subjects had known malformations. Craniospinal AVMs are sufficiently uncommon, even in tertiary referral centers, so that acquisition of a large anatomically homogeneous group would be challenging. To this end, we regard our results as preliminary and indicative of the potential of CE-MRA at 3T.

Conclusion

A combination of time-resolved and high-spatial-resolution 3D CE-MRA at 3T can provide reliable anatomic and functional information about craniospinal AVMs. Our preliminary study showed close concordance between CE-MRA and CCA, suggesting that in select cases, follow-up CCA may be avoided or minimized. Further work will be required to validate our findings in larger patient cohorts.

References

1. Mast H, Young WL, Koennecke HC, et al. **Risk of spontaneous haemorrhage after diagnosis of cerebral arteriovenous malformation.** *Lancet* 1997;350:1065–68
2. Ondra SL, Troupp H, George ED, et al. **The natural history of symptomatic arteriovenous malformations of the brain: a 24-year follow-up assessment.** *J Neurosurg* 1990;73:387–91
3. Graf CJ, Perret GE, Torner JC. **Bleeding from cerebral arteriovenous malformations as part of their natural history.** *J Neurosurg* 1983;58:331–37
4. Wilkins RH. **Natural history of intracranial vascular malformations: a review.** *Neurosurgery* 1985;16:421–30
5. Hartmann A, Mast H, Mohr JP, et al. **Morbidity of intracranial hemorrhage in patients with cerebral arteriovenous malformation.** *Stroke* 1998;29:931–34
6. Luessenhop AJ, Rosa L. **Cerebral arteriovenous malformations: indications for and results of surgery, and the role of intravascular techniques.** *J Neurosurg* 1984;60:14–22
7. Kader A, Young WL, Pile-Spellman J, et al. **The influence of hemodynamic and anatomic factors on hemorrhage from cerebral arteriovenous malformations.** *Neurosurgery* 1994;34:801–07, discussion 807–08
8. Spetzler RF, Hargraves RW, McCormick PW, et al. **Relationship of perfusion pressure and size to risk of hemorrhage from arteriovenous malformations.** *J Neurosurg* 1992;76:918–23
9. Marks MP, Lane B, Steinberg GK, et al. **Hemorrhage in intracerebral arteriovenous malformations: angiographic determinants.** *Radiology* 1990;176:807–13
10. Redekop G, TerBrugge K, Montanera W, et al. **Arterial aneurysms associated with cerebral arteriovenous malformations: classification, incidence, and risk of hemorrhage.** *J Neurosurg* 1998;89:539–46
11. Hankey GJ, Warlow CP, Sellar RJ. **Cerebral angiographic risk in mild cerebrovascular disease.** *Stroke* 1990;21:209–22
12. Willinsky RA, Taylor SM, TerBrugge K, et al. **Neurologic complications of cerebral angiography: prospective analysis of 2,899 procedures and review of the literature.** *Radiology* 2003;227:522–28
13. Dion JE, Gates PC, Fox AJ, et al. **Clinical events following neuroangiography: a prospective study.** *Stroke* 1987;18:997–1004
14. Nael K, Villablanca JP, Saleh R, et al. **Contrast-enhanced MR angiography at 3T in the evaluation of intracranial aneurysms: a comparison with time-of-flight MR angiography.** *AJNR Am J Neuroradiol* 2006;27:2118–21
15. Nael K, Ruehm SG, Michaely HJ, et al. **High spatial-resolution CE-MRA of the carotid circulation with parallel imaging: comparison of image quality between 2 different acceleration factors at 3.0 Tesla.** *Invest Radiol* 2006;41:391–99
16. Nael K, Fenchel M, Salamon N, et al. **Three-dimensional cerebral contrast-enhanced magnetic resonance venography at 3.0 Tesla: initial results using highly accelerated parallel acquisition.** *Invest Radiol* 2006;41:763–68
17. Nael K, Michaely HJ, Villablanca P, et al. **Time-resolved contrast enhanced magnetic resonance angiography of the head and neck at 3.0 Tesla: initial results.** *Invest Radiol* 2006;41:116–24
18. Fenchel M, Nael K, Ruehm S, et al. **Isotropic high spatial resolution magnetic resonance angiography of the supra-aortic arteries using two-dimensional parallel imaging (iPAT2) at 3 Tesla: a feasibility study.** *Invest Radiol* 2006;41:545–52
19. Carr JC, Ma J, Desphande V, et al. **High-resolution breath-hold contrast-enhanced MR angiography of the entire carotid circulation.** *AJR Am J Roentgenol* 2002;178:543–49
20. Cognard C, Casasco A, Toevi M, et al. **Dural arteriovenous fistulas as a cause of intracranial hypertension due to impairment of cranial venous outflow.** *J Neurol Neurosurg Psychiatry* 1998;65:308–16
21. Collice M, D'Aliberti G, Talamonti G, et al. **Surgical interruption of leptomeningeal drainage as treatment for intracranial dural arteriovenous fistulas without dural sinus drainage.** *J Neurosurg* 1996;84:810–17
22. Duffau H, Lopes M, Janosevic V, et al. **Early rebleeding from intracranial dural arteriovenous fistulas: report of 20 cases and review of the literature.** *J Neurosurg* 1999;90:78–84
23. Lopes M, Duffau H, Fleuridas G. **Primary spheno-orbital angiosarcoma: case report and review of the literature.** *Neurosurgery* 1999;44:405–07, discussion 407–08
24. Thompson BG, Doppman JL, Oldfield EH. **Treatment of cranial dural arteriovenous fistulae by interruption of leptomeningeal venous drainage.** *J Neurosurg* 1994;80:617–23
25. da Costa LB, Terbrugge K, Farb R, et al. **Surgical disconnection of cortical venous reflux as a treatment for Borden type II dural arteriovenous fistulae.** *Acta Neurochir (Wien)* 2007;149:1103–08. Epub 2007 Oct 3
26. Davies MA, TerBrugge K, Willinsky R, et al. **The validity of classification for the clinical presentation of intracranial dural arteriovenous fistulas.** *J Neurosurg* 1996;85:830–37
27. Satomi J, van Dijk JM, Terbrugge KG, et al. **Benign cranial dural arteriovenous fistulas: outcome of conservative management based on the natural history of the lesion.** *J Neurosurg* 2002;97:767–70
28. Van Dijk JM, TerBrugge KG, Willinsky RA, et al. **Multidisciplinary management of spinal dural arteriovenous fistulas: clinical presentation and long-term follow-up in 49 patients.** *Stroke* 2002;33:1578–83
29. Stiver SI, Ogilvy CS. **Micro-arteriovenous malformations: significant hemorrhage from small arteriovenous shunts.** *Neurosurgery* 2000;46:811–18, discussion 818–19
30. Margolis G, Odom GL, Woodhall B, et al. **The role of small angiomatous malformations in the production of intracerebral hematomas.** *J Neurosurg* 1951;8:564–75
31. Warren DJ, Hoggard N, Walton L, et al. **Cerebral arteriovenous malformations: comparison of novel magnetic resonance angiographic techniques and conventional catheter angiography.** *Neurosurgery* 2001;48:973–82, discussion 982–83
32. Unlu E, Temizoz O, Albayram S, et al. **Contrast-enhanced MR 3D angiography in the assessment of brain AVMs.** *Eur J Radiol* 2006;60:367–78
33. Meckel S, Maier M, Ruiz DS, et al. **MR angiography of dural arteriovenous fistulas: diagnosis and follow-up after treatment using a time-resolved 3D contrast-enhanced technique.** *AJNR Am J Neuroradiol* 2007;28:877–84
34. Batjer H, Suss RA, Samson D. **Intracranial arteriovenous malformations associated with aneurysms.** *Neurosurgery* 1986;18:29–35
35. Perret G, Nishioka H. **Report on the cooperative study of intracranial aneurysms and subarachnoid hemorrhage. Section VI. Arteriovenous malformations: an analysis of 545 cases of cranio-cerebral arteriovenous malformations and fistulae reported to the cooperative study.** *J Neurosurg* 1966;25:467–90
36. Nagaraja S, Capener D, Coley SC, et al. **Brain arteriovenous malformations: measurement of nidal volume using a combination of static and dynamic magnetic resonance angiography techniques.** *Neuroradiology* 2005;47:387–92